

Study of Effects of Stratification on the Wake Behind the SUBOFF Bare Hull at $Re=1.2 \times 10^7$

Gang Gao¹, Yangjun Wang², Liushuai Cao¹, Decheng Wan^{1*}

¹ Computational Marine Hydrodynamics Lab (CMHL), School of Naval Architecture, Ocean and Civil Engineering, Shanghai Jiao Tong University, Shanghai, China

² College of Advanced Interdisciplinary Studies, National University of Defense Technology, Nanjing, China

*Corresponding Author

ABSTRACT

For submarines, at the model scale, it is rare to simultaneously consider the effects of high Reynolds numbers and stratified flow on the wake. In this study, numerical simulations of the wake of the SUBOFF bare hull are conducted under Reynolds number ($Re = 1.2 \times 10^7$) and Froude numbers ($Fr = 1, 2, 3, \infty$), where $Fr = \infty$ represents the unstratified (UNS) condition. The simulations are based on the Boussinesq approximation and the large eddy simulation (LES) method. At high Reynolds number, the effects of varying Froude numbers on velocity deficit, root mean square (RMS) values, internal waves, and turbulent kinetic energy (TKE) in the wake are investigated. The results reveal that the wake evolves through two stages: the three-dimensional (3D) stage and the non-equilibrium (NEQ) stage. In the NEQ stage, as the Froude number increases, the velocity deficit along the wake centerline decreases, indicating a shorter lifespan of the wake. Conversely, as the Froude number decreases, the vertical suppression of wake vortex structures becomes more significant, while the horizontal extent of the wake expands. The RMS values of velocity components exhibit clear anisotropy, and the horizontal distribution of internal waves gradually increases. Additionally, the TKE in the wake diminishes, and spatial distribution demonstrates pronounced anisotropy, appearing compressed vertically and stretched horizontally.

KEY WORDS: Stratified flow; SUBOFF; numerical investigation; wake; velocity deficit; large eddy simulation

INTRODUCTION

A submarine, as a representative of underwater navigation, is a critical piece of strategic equipment in military competition among major powers. When navigating in the ocean, a submarine generates a complex wake that persists for a significant duration and has far-reaching effects. These wake characteristics are crucial indicators of stealth performance, making them a focal point of research for maritime powers. The relationship between wake of submarine and its stealth capabilities has become a prominent topic in non-acoustic submarine detection and has garnered considerable attention from researchers worldwide (Cao et al. 2023).

Current research on submarine wakes, both domestically and

internationally, primarily focuses on experimental studies and numerical simulations. Huang et al. (1992) conducted tests on eight basic models using the DARPA SUBOFF bare hull in wind tunnels and tanks. These experiments provided data on surface pressure distributions, boundary layer velocity profiles, wake flow characteristics, and the effects of different appendages on wake flow for various models. Their experimental results established a database that has since been widely used by researchers for CFD validation and flow mechanism analysis. Zheng et al. (2023) measured the towing force, lateral force, and moment acting on the SJTU-BX01 submarine model at various water flow velocities and depths in tank and focused on the hydrodynamic performance of the submarine at different depths and Froude numbers, their results indicated that turbulent boundary layer separation at the tail of submarine occurred earlier when the submarine was closer to the water surface, while flow stability improved as the submarine moved farther from the surface.

Gross et al. (2015) investigated the flow around a hemisphere-cylinder geometry using a hybrid RANS/LES turbulence model, and analyzed three-dimensional flow separation under various angles of attack ($\alpha = 10^\circ, 30^\circ$) and Reynolds numbers ranging from 5×10^3 to 5×10^5 , the results showed that at an angle of attack of 30° , leeward vortices formed. Gross et al. (2012) also employed the direct numerical simulation (DNS) method to investigate flow separation phenomena for two geometries: the DARPA SUBOFF bare hull model ($Re = 10000 - 20000$, $\alpha = 10^\circ, 30^\circ$) and the hemispherical-cylinder geometry ($Re = 2000 - 5000$, $\alpha = 10^\circ, 30^\circ$). Their study revealed that at $\alpha = 30^\circ$, a convective vortex formed on the leeward side. Furthermore, as the Reynolds number increased, flow instability and the development of small-scale structures became more pronounced.

Posa et al. (2016) employed high-resolution wall-modeled large eddy simulation (WMLES) combined with a semi-implicit time-stepping method to investigate flow characteristics, at $Re = 1.2 \times 10^6$ and an angle of attack of 0° , they found that, compared to the command tower, the shear layer at the trailing edge of the appendage and the turbulent boundary layer at the tail of model had a greater influence on the wake, the turbulent stress in the wake exhibited a bimodal distribution, which was further amplified by the presence of the appendage. Additionally, the interaction between the appendage and the command tower increased the

turbulence intensity in the wake. Posa et al. (2020) also analyzed the effects of Reynolds numbers ($Re = 1.2 \times 10^6, 1.2 \times 10^7$) on the turbulent boundary layer and wake characteristics, they revealed that the thickness of the tail boundary layer of the DARPA SUBOFF model decreases with increasing Reynolds number, additionally, as the Reynolds number increases, the peak turbulent kinetic energy (TKE) in the wake decreases, its distribution becomes more uniform, and the TKE distribution gradually approaches axisymmetry. Jiang et al. (2024) utilized the Large Eddy Simulation (LES) method with wall modeling (WMLES) and the Finite Volume Method (FVM) for third-order reconstruction (FVMS3) to calculate turbulent noise at high Reynolds numbers ($Re = 1.2 \times 10^7$), and found that the pressure fluctuations on the wall exhibited a low-frequency broadband spectrum, with energy primarily concentrated in the low-frequency range.

Previous studies have primarily focused on unstratified flow, with limited attention given to stratified flow. However, a key characteristic of the actual marine environment is stratification, where the physical properties of seawater, such as temperature and density, vary with depth. Wake behavior in stratified flow differs significantly from that in unstratified flow. Research methods for studying stratified flow are predominantly based on experiments and numerical simulations (Cao et al. 2024).

Spedding et al. (1997) measured the velocity field and turbulence characteristics in the wake behind a sphere using high-precision digital particle image velocimetry (DPIV) in a stratified water channel. They proposed that the evolution of the wake can be divided into three stages: the three-dimensional turbulence stage (3D), the non-equilibrium stage (NEQ), and the quasi-two-dimensional stage (Q2D). Bonnie et al. (2002) utilized digital particle image velocimetry (DPIV) to measure velocity and vorticity distributions in a linearly stratified saltwater environment. They concluded that the evolution of the wake can be divided into four distinct stages: the near-wake region, collapse region, transition region, and far-wake region.

Pal et al. (2017) employed direct numerical simulation (DNS) methods to investigate the wake characteristics of a sphere in a stratified flow. Their study revealed that the wake evolution can be divided into three stages: the near-wake region, the non-equilibrium region (NEQ), and the quasi-two-dimensional region (Q2D), the velocity deficit along the centerline of the wake follows $u \sim x^{-0.25}$ in the NEQ stage and $u \sim x^{-0.76}$ in the Q2D stage, additionally, it was found that stratification significantly enhances the anisotropy of the flow field. Chen et al. (2021) investigated the temperature and salinity variations in the wake of a full-scale submarine in a stratified flow using large eddy simulation (LES). They found that the degree of temperature and salinity disturbance was positively correlated with the velocity of submarine. In the near-wake region, strong mixing of temperature and salinity occurred within the wake, whereas in the far-wake region, the vortex structure gradually weakened.

Huang et al. (2022) compared the flow characteristics of submarine wakes in unstratified and stratified flows using the RANS method and the SST $k-\omega$ turbulence model on a full-scale Joubert BB2 submarine. They revealed that in stratified flow, the resistance of submarine increased by 5.5%, while the height and width of the wake decreased, exhibiting significant anisotropy. In our earlier work, Gao et al. (2024) focused on underwater vehicles and employed large eddy simulation (LES) to analyze the effects of the Froude number, depth, and density ratio of a two-layer fluid on the free surface and inner interface, this research provided a foundation for subsequent numerical simulations of linearly stratified flow.

For submarines, most current research at high Reynolds numbers is conducted in unstratified flow, with limited attention given to stratified

flow. Studies in stratified flow primarily focus on simple geometric bodies, such as spheres, or full-scale submarines. However, it is rare to simultaneously consider both high Reynolds numbers and stratified flow at the model scale. Therefore, it is essential to conduct corresponding numerical simulations to address this gap.

This study employs the large eddy simulation (LES) method and Boussinesq approximation to approximate the stratified flow of submarines at the model scale and high Reynolds numbers. The primary focus is on examining the effects of the Froude number on velocity deficit, vortex structure, internal waves, turbulent kinetic energy, and other wake characteristics. The structure of the article is organized as follows: first, the governing equations for the numerical simulation are presented. Next, the submarine model, computational domain, and boundary condition settings are introduced. Subsequently, grid sensitivity analysis and method validation are performed. Finally, the results of the numerical simulation are discussed and analyzed.

NUMERICAL METHODS

Governing Equation

Numerical simulations in this study are conducted using the commercial software STAR-CCM+ 2023, a widely used multiphysics platform. The Large Eddy Simulation (LES) method is employed under the Boussinesq approximation, solving the spatially filtered governing equations. To model subgrid-scale (SGS) turbulence, this study adopts the Wall-Adapting Local Eddy-viscosity (WALE) model, which is particularly effective for resolving near-wall turbulence in stratified flows. Compared with other SGS models, such as the Smagorinsky and dynamic Smagorinsky models, the WALE model offers improved accuracy for complex boundary conditions. The governing equations in dimensionless form are provided as follows.

Mass:

$$\frac{\partial u_i}{\partial x_i} = 0 \quad (1)$$

Momentum:

$$\frac{\partial u_i}{\partial t} + u_j \frac{\partial u_i}{\partial x_j} = -\frac{\partial p}{\partial x_i} + \frac{1}{Re} \frac{\partial}{\partial x_j} \left[\left(1 + \frac{\nu_{sgs}}{\nu} \right) \frac{\partial u_i}{\partial x_j} \right] - \frac{1}{Fr^2} \rho_d \delta_{i3} \quad (2)$$

Density:

$$\frac{\partial \rho}{\partial t} + u_j \frac{\partial \rho}{\partial x_j} = \frac{1}{Re} \frac{\partial}{\partial x_j} \left[\left(1 + \frac{\nu_{sgs}}{\nu} \right) \frac{\partial \rho}{\partial x_j} \right] \quad (3)$$

Where Fr and Re represent, respectively, Froude numbers and Reynolds numbers. u_i and x_i represent velocity and position in different directions, respectively. The terms ρ_d , δ_{i3} , ν_{sgs} , ν and p denote, respectively, the density fluctuation relative to the background density, the Kronecker delta, the subgrid-scale viscosity, the constant kinematic viscosity, and the filtered pressure.

Numerical Scheme

The numerical simulation adopts the SIMPLE algorithm, utilizes first-order time discretization, and employs an implicit unsteady solver for unsteady flow. Additionally, the Segregated Flow model is used to

simulate complex flows. A time step of 0.002s is chosen to ensure that the Courant number remains less than 1.

NUMERICAL VALIDATION

Geometric Model

As shown in Figure 1, the geometric model used in this study is the SUBOFF model, designed by the US Navy Laboratory. The model is a rotational body composed of three sections: an arc-shaped head, a cylindrical middle section, and a tapered tail section. L represents the total length of the model, which is 4.356 m, and D represents its diameter, which is 0.508 m.

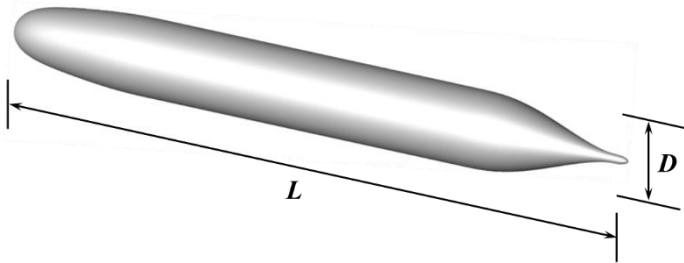


Fig. 1. Geometric model

Simulation Setup and Boundary Setting

As shown in Figure 2, the bow of the SUBOFF model is taken as the coordinate origin. The computational domain is defined with the following dimensions: to prevent flow reflection caused by close proximity, the distance from the inlet of domain to the bow of the SUBOFF is $20D$, the distance from the outlet to the stern is $57D$, the SUBOFF model has an aspect ratio of 8.575, with a distance of $65D$ from the bow to the outlet of the computational domain, the distance from the left and right boundaries to the SUBOFF axis is $10D$, and the distance from the upper and lower boundaries to the axis is $5D$. The inlet of the computational domain is defined as a velocity inlet, the outlet is set as a outlet, and the left, right, upper, and lower boundaries are all specified as velocity inlets. For the surface of geometric object, no-slip wall boundary condition is applied.

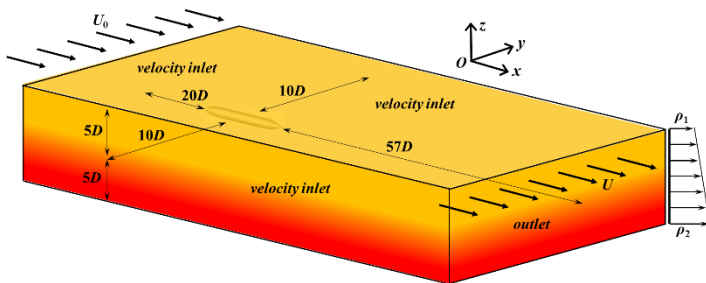


Fig. 2. Computational domain

Grid Generation

As shown in Figures 3 and 4, an unstructured grid is used to discretize the surface and flow field surrounding the SUBOFF model. The grid near the SUBOFF surface is refined to accurately capture the flow characteristics of the boundary layer, while the grid size is gradually coarsened in regions farther away from the model to reduce computational complexity. Additionally, the grid is further refined in the tail and rear wake regions of the SUBOFF to finely simulate the wake evolution process.

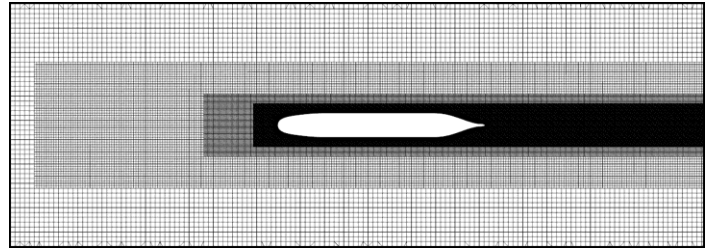


Fig. 3. Computational mesh (overall view)

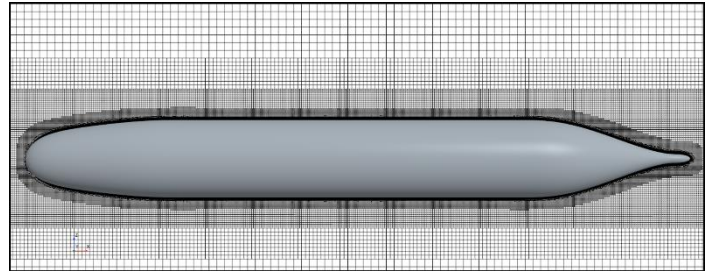


Fig. 4. Computational mesh (enlarged view)

Validation and Verification

A sensitivity analysis of the grid is first conducted using three grid resolutions: coarse, medium, and fine, with grid sizes of 11 million, 18 million, and 30 million cells, respectively. In STAR-CCM+ 2023, these grid resolutions are controlled by varying the basic size, which differed by factors of 1.2. Numerical simulations are performed for all three grids, focusing on the velocity deficit along the centerline of the wake and the pressure coefficient distribution on the SUBOFF surface, as shown in Figures 5 and 6. The results indicate that the pressure coefficient distribution remains consistent across all grids. However, for the velocity deficit along the centerline of the wake, the medium and fine grids produced similar results, while the coarse grid showed significant deviations. To balance computational cost and accuracy, the medium grid is selected for subsequent simulations.

As shown in Figure 7, validation of the numerical method is conducted by comparing the pressure coefficient distribution on the SUBOFF surface with the results of Huang et al. (1992). The comparison shows close agreement over most regions of the hull surface, demonstrating the accuracy of the numerical simulation method employed in this study.

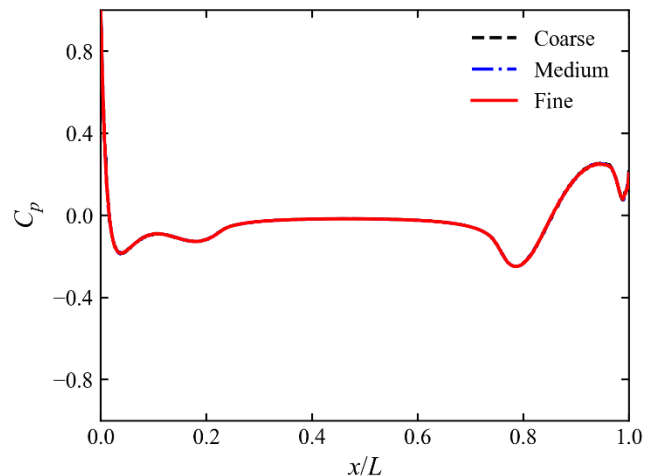


Fig. 5. The mean surface pressure coefficients with different grid

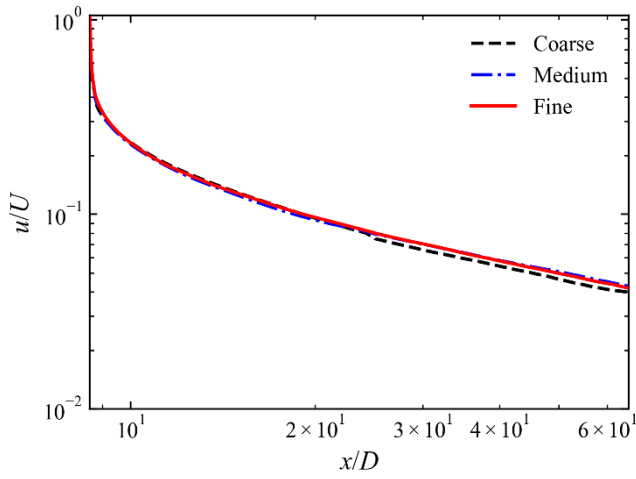


Fig. 6. The normalized velocity deficit with different grid

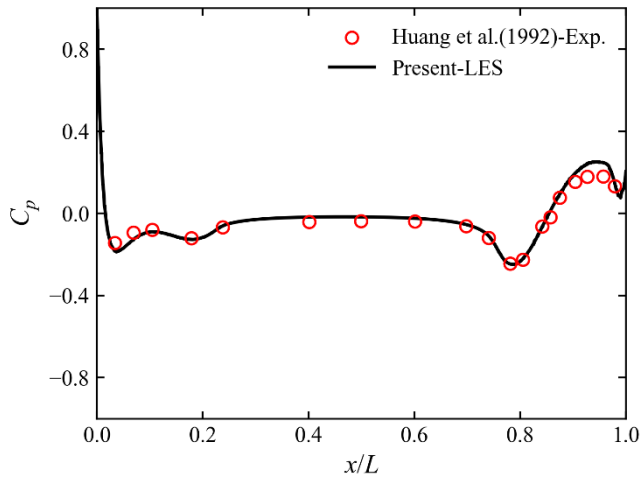


Fig. 7. The mean surface pressure coefficients

RESULTS AND DISCUSSION

Firstly, several dimensionless parameters required for the numerical simulation are introduced. The Reynolds number is defined as shown in Equation (4), and the Froude number is given in Equation (5), where U , D , and ν represent the characteristic velocity, characteristic length, and dynamic viscosity of the fluid, respectively. The buoyancy frequency, N , is defined in Equation (6). The Prandtl number is expressed in Equation (7), where ν and α denote the momentum diffusion rate and heat diffusion rate of the fluid, respectively.

The main parameters used for the numerical simulation in this study are listed in Table 1. The Prandtl number and Reynolds number remain constant, while the influence of different Froude numbers on the wake is the primary focus, where $Fr = \infty$, represents unstratified flow. Based on the study by Stadler et al. (2010), the Prandtl number is set to 1. And the Reynolds number is defined as $Re = 1.2 \times 10^7$. The Reynolds number is selected due to the availability of experimental data for method validation and because such high Reynolds numbers are rarely considered in stratified flow research.

It is worth noting that, due to the large aspect ratio of the SUBOFF geometry, the characteristic length can be defined as either the length L or the diameter D of the model. In this study, the Reynolds number and Froude number are defined based on the length L , and are denoted as Re_L

and Fr_L , respectively.

$$Re = \frac{UD}{\nu} \quad (4)$$

$$Fr = \frac{U}{ND} \quad (5)$$

$$N = \sqrt{\frac{g}{\rho_0} \frac{d\rho}{dz}} \quad (6)$$

$$Pr = \frac{\nu}{\alpha} \quad (7)$$

Table 1. Computational cases

Case	Fr	Pr	Re
1	1	1	1.2×10^7
2	2	1	1.2×10^7
3	3	1	1.2×10^7
4	∞	1	1.2×10^7

The velocity deficit

Figure 8 illustrates the normalized velocity deficit along the wake centerline. As the Froude number (Fr) decreases, the stratification intensifies, leading to an increase in velocity deficit and a slower rate of decay. When $Fr = 1$, the velocity deficit decreases to a local minimum, marking the first region of the wake, known as the three-dimensional region (3D), where buoyancy effects are relatively weak. Beyond this position, the velocity deficit gradually changes, entering the second region of the wake, referred to as the non-equilibrium region (NEQ), where buoyancy effects become more pronounced. At higher Froude numbers ($Fr = 2$ and $Fr = 3$), stratification weakens, and no local minimum is observed as seen with $Fr = 1$. For $Fr = \infty$, the decay rate increases significantly. These observations suggest that stratified flow can prolong the lifespan of wake by reducing the rate of velocity decay.

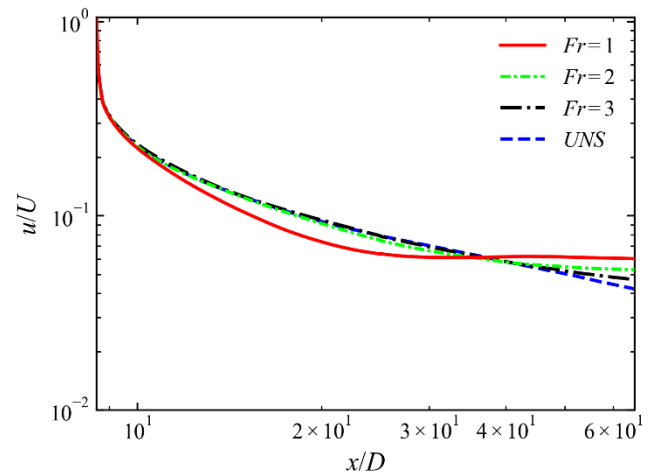


Fig. 8. The normalized velocity deficit along the wake centerline

The vortex structure under different Froude numbers is analyzed using the Q -criterion method, as illustrated in Figure 9. The vortex structures are visualized with flow velocity (u_x/U) as the scalar field. At $Fr = 1$, strong stratification significantly suppresses the vortex structure in the vertical direction in regions far from the SUBOFF body, leading to vertically flattened and horizontally extended vortices. The vortex structure exhibits pronounced anisotropy. At $Fr = 2$ and $Fr = 3$, the stratification weakens, resulting in a reduced vertical suppression effect on the vortex structure and a notable decrease in anisotropy. At $Fr = \infty$, the wake vortex structure transitions to a fully three-dimensional configuration, with vortices evenly distributed in both vertical and horizontal directions, and the anisotropy is significantly diminished. Overall, the vortex structures reveal that as the Froude number increases, the wake evolves from a predominantly two-dimensional structure to a fully three-dimensional.

$$\text{div}_h = \frac{\partial u}{\partial x} + \frac{\partial v}{\partial y} \quad (8)$$

In unstratified flow, although density stratification is absent, a horizontal velocity field still exists. Therefore, the divergence of the horizontal velocity field is also calculated under unstratified conditions. While the physical interpretation of the divergence values differs from those in stratified flow, this approach serves as an effective method for comparing unstratified and stratified flow. Figure 10 compares internal waves at $z = 0$ under different Froude numbers (Fr). As the Froude number decreases, distinct striped patterns emerge, characterized by periodic expansion and contraction, with alternating positive and negative divergence distributions. Conversely, as the Froude number increases, the stratification weakens, vertical mixing intensifies, and the horizontal range of divergence distribution significantly diminishes. At $Fr = \infty$, the divergence values are notably reduced, and the striped patterns disappear. In the case of uniform flow, the divergence values are primarily influenced by the inherent vortex structures.

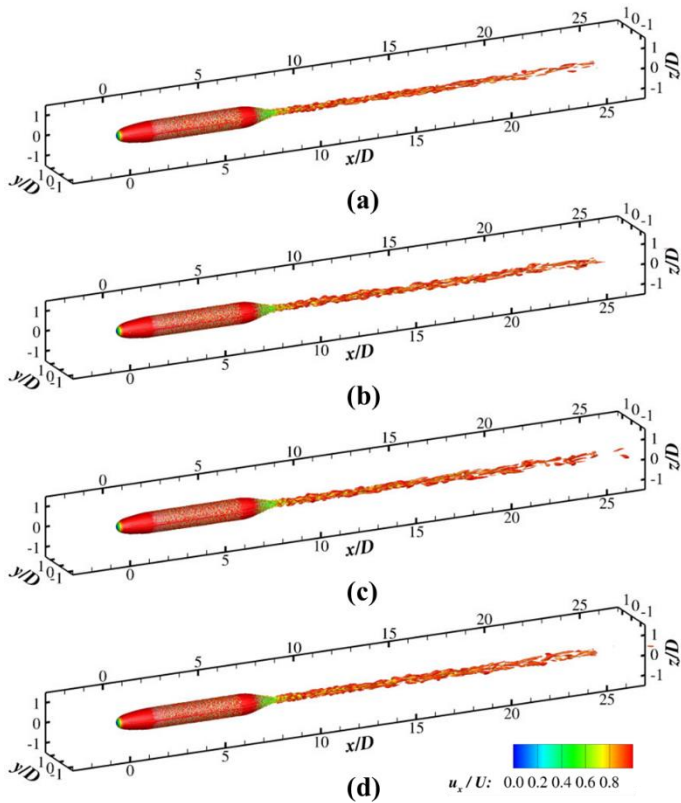


Fig. 9. Vortex structure at different Froude Number ($Q = 1$). (a) $Fr = 1$; (b) $Fr = 2$; (c) $Fr = 3$; (d) $Fr = \infty$

Internal waves

The generation of internal waves requires two key conditions: the presence of disturbance sources and density stratification. The propagation of internal waves is governed by density gradients. Research of Spedding et al. (2014) suggests that the divergence of the horizontal velocity field can be employed to identify internal waves, as expressed in Equation (8). By calculating this divergence, its positive and negative values correspond to the expansion and contraction of the fluid in the horizontal plane, respectively. Specifically, when $\text{div}_h > 0$, it indicates fluid expansion in the horizontal plane, whereas $\text{div}_h < 0$ signifies fluid contraction. The full velocity divergence in three dimensions satisfies continuity equation, in stratified flow, vertical velocity variations compensate for changes in the horizontal divergence.

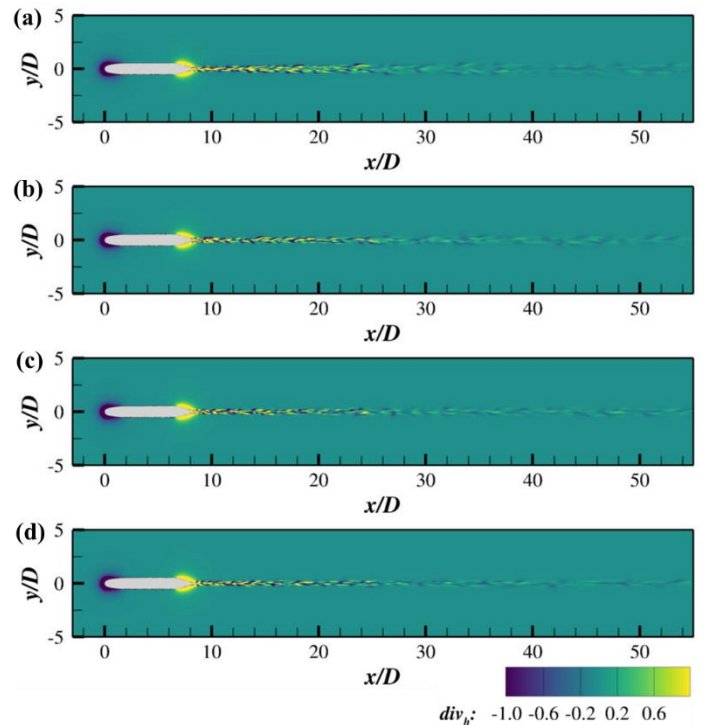


Fig. 10. The contour of internal waves at $z = 0$. (a) $Fr = 1$; (b) $Fr = 2$; (c) $Fr = 3$; (d) $Fr = \infty$

Turbulence levels

The root mean square (RMS) values of velocity components in different directions, as well as the RMS values of density, are computed. Figures 11–14 illustrate these results. The RMS values of the velocity components are non-dimensionalized using the flow velocity, while Δ_{bg} , representing the density difference between the upper and lower boundaries of the computational domain, is used to non-dimensionalize the RMS values of density.

For the root mean square (RMS) value of flow velocity, the results show that when $x/D < 27$, the RMS value decreases with increasing Froude number (Fr), although the rate of decrease slows down. In contrast, when $x/D > 27$, the RMS value gradually increases with Fr . For the spanwise and vertical velocity components, the RMS values increase as Fr

increases. However, at $Fr = 1$, the RMS of vertical velocity exhibits periodic fluctuations in both directions, a phenomenon not observed in the streamwise and spanwise velocity components. This indicates that stratification primarily impacts the vertical velocity component. Regarding the RMS variation of density, the largest density fluctuations and peak values occur at $Fr = 1$, accompanied by the fastest attenuation.

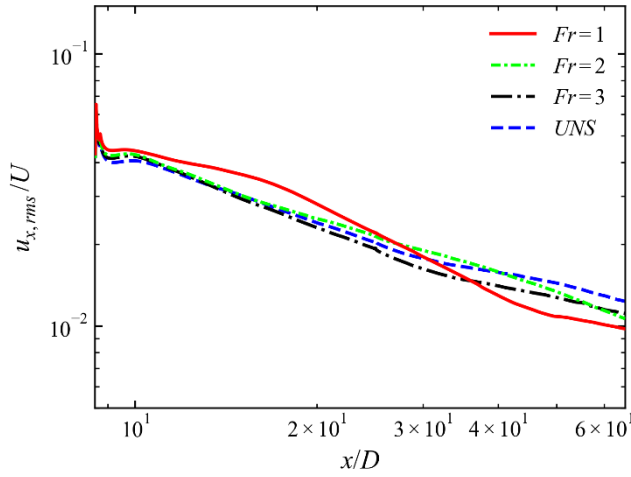


Fig. 11. Root mean square value of streamwise velocity

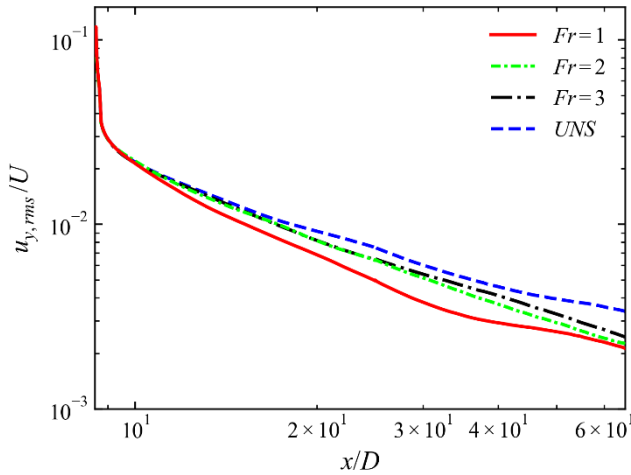


Fig. 12. Root mean square value of lateral velocity

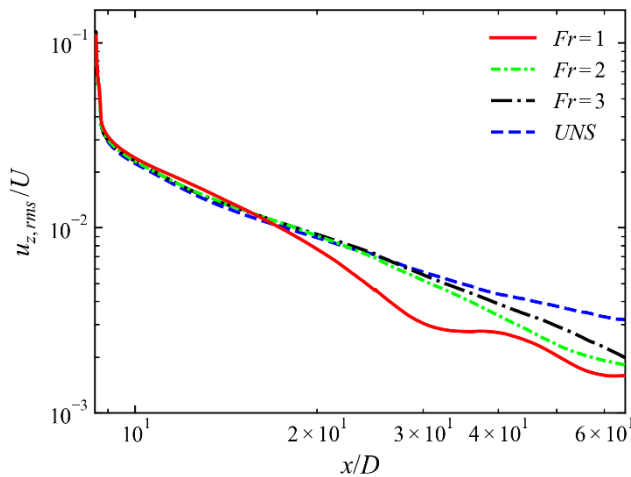


Fig. 13. Root mean square value of vertical velocity

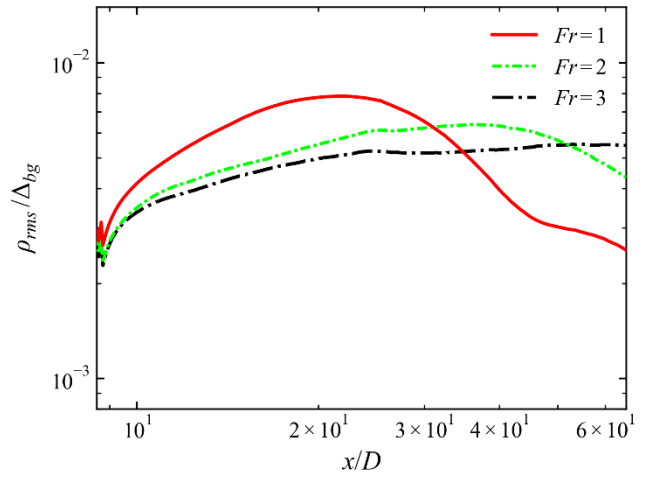


Fig. 14. Root mean square value of density

Turbulent kinetic energy

Figure 14 shows the area-integrated turbulent kinetic energy (TKE) at different positions in the SUBOFF wake. In studies of wake in sphere, the area-integrated TKE initially increases to a peak and then gradually decreases. However, in contrast to wake in sphere, the area-integrated TKE in the SUBOFF wake decreases consistently across different Froude numbers (Fr). In the near-wake region, the area-integrated TKE values are nearly identical for different Fr , indicating that momentum dominates in this region. As the distance increases and Fr decreases, the area-integrated TKE decays more rapidly, suggesting that enhanced stratification suppresses turbulence generation. When $Fr = \infty$, where no density gradient is present, the wake undergoes strong mixing, allowing turbulence to persist for a longer duration.

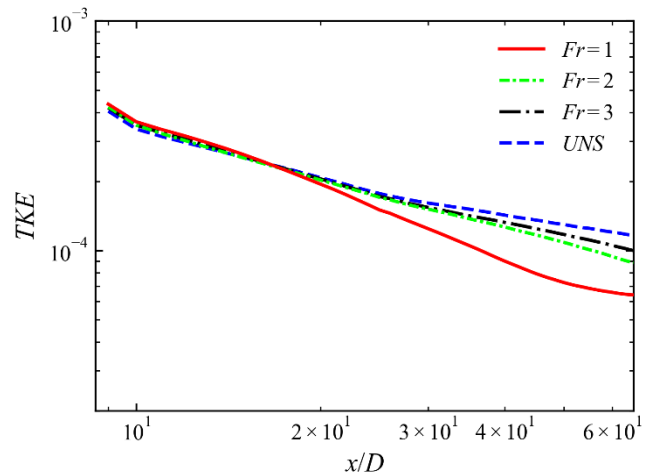


Fig. 15. Area integrated turbulent kinetic energy for different Froude numbers

Similarly, the turbulent kinetic energy (TKE) distribution in the wake at different Froude numbers (Fr) and positions is analyzed, as shown in Figure 15. When the positions are close to the body, the TKE distribution at various Fr values exhibits a similar circular shape and is isotropic in all directions. As the distance increases and Fr decreases, the TKE distribution transitions from a circular shape to a spindle-like structure that is vertically compressed and horizontally extended. For $Fr = \infty$, the TKE distribution remains isotropic in all directions.

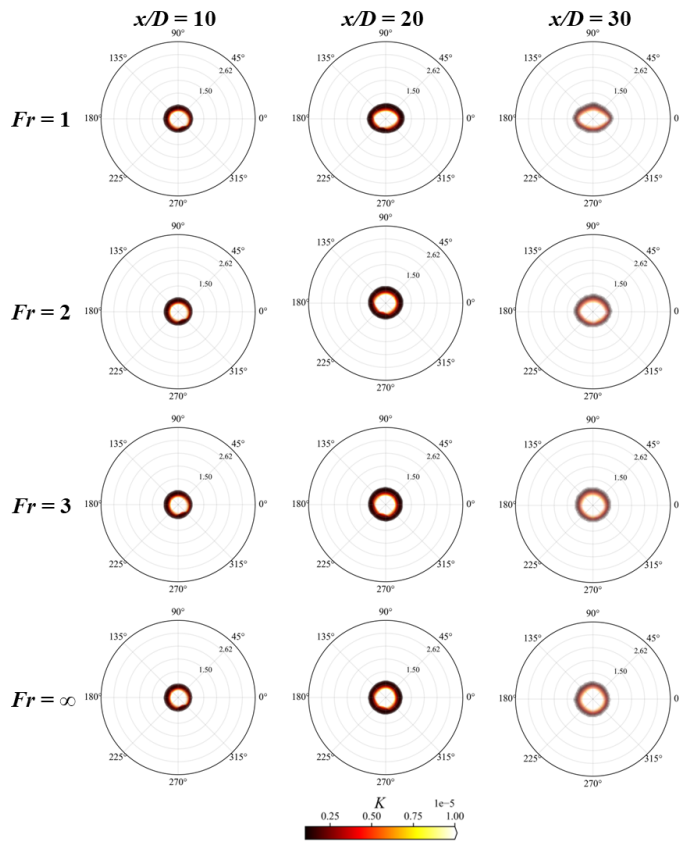


Fig. 16. Distribution of turbulent kinetic energy

CONCLUSIONS

In this study, the simulations are based on the Boussinesq approximation and the large eddy simulation (LES) method. At high Reynolds numbers, the effects of varying Froude numbers on velocity deficit, root mean square (RMS) values, internal waves, and turbulent kinetic energy (TKE) in the wake are investigated.

(a) As the Froude number (Fr) decreases, the velocity deficit decays more slowly, leading to a longer wake lifespan. At $Fr = 1$, the wake can be characterized by two distinct stages: the three-dimensional region and the non-equilibrium region.

(b) As the Froude number (Fr) decreases, the vortex structure becomes increasingly suppressed in the vertical direction, while its distribution and the divergence values expand significantly in the horizontal direction. The divergence distribution exhibits distinct striped patterns, characterized by periodic expansion and contraction with alternating positive and negative divergence values.

(c) As the Froude number (Fr) decreases, the root mean square (RMS) values of velocity components in all directions diminish, the area-integrated turbulent energy gradually decreases, and the turbulent energy distribution exhibits pronounced anisotropy, forming a spindle-like shape that is vertically compressed and horizontally extended.

ACKNOWLEDGMENTS

This work is supported by the National Natural Science Foundation of China (52131102), to which the authors are most grateful.

REFERENCES

- Bonnier, M., & Eiff, O. (2002). Experimental investigation of the collapse of a turbulent wake in a stably stratified fluid. *Physics of fluids*, 14(2), 791-801.
- Cao, L. S., Gao, G., Guo, E. K., & Wan, D. C. (2023). Hydrodynamic performances and wakes induced by a generic submarine operating near the free surface in continuously stratified fluid. *Journal of Hydrodynamics*, 35(3), 396-406.
- Cao, L., Pan, Y., Gao, G., Li, L., & Wan, D. (2024). Review on the Hydro-and Thermo-Dynamic Wakes of Underwater Vehicles in Linearly Stratified Fluid. *Journal of Marine Science and Engineering*, 12(3), 490.
- Chen, Q., Lin, Q., Xuan, Y., & Han, Y. (2021). Investigation on the thermohaline structure of the stratified wake generated by a propagating submarine. *International Journal of Heat and Mass Transfer*, 166, 120808.
- De Stadler, M. B., Sarkar, S., & Brucker, K. A. (2010). Effect of the Prandtl number on a stratified turbulent wake. *Physics of Fluids*, 22(9).
- Gao, G., Pan, Y., Wang, Y., Shen, Z., Cao, L., & Wan, D. (2024). Evolution and propagation characteristics of the wake induced by an underwater vehicle moving in two layers of fluid: A parametric study. *Physics of Fluids*, 36(11).
- Gross, A., & Fasel, H. F. (2015). Hybrid turbulence model simulations of hemisphere-cylinder geometry. *International Journal of Heat and Fluid Flow*, 54, 28-38.
- Gross, A., Jagadeesh, C., & Fasel, H. (2012). Numerical investigation of three-dimensional separation on axisymmetric bodies at angle of attack. *In 50th AIAA Aerospace Sciences Meeting including the New Horizons Forum and Aerospace Exposition* (p. 97).
- Huang, F., Meng, Q., Cao, L., & Wan, D. (2022). Wakes and free surface signatures of a generic submarine in the homogeneous and linearly stratified fluid. *Ocean Engineering*, 250, 111062.
- Huang, T., Liu, H.L., Groves, N.C., Forlini, T., Blanton, J., Gowing, S., 1992. Measurements of flows over an axisymmetric body with various appendages in a wind tunnel: The DARPA SUBOFF experimental program, in: *In Proceedings of the 19th Symposium on Naval Hydrodynamics*.
- Jiang, P., Liao, S., & Xie, B. (2024). Large-eddy simulation of hydrodynamic noise from turbulent flows past an axisymmetric hull using high-order schemes. *arXiv preprint arXiv:2407.10475*.
- Pal, A., Sarkar, S., Posa, A., & Balaras, E. (2017). Direct numerical simulation of stratified flow past a sphere at a subcritical Reynolds number of 3700 and moderate Froude number. *Journal of Fluid Mechanics*, 826, 5-31.
- Posa, A., & Balaras, E. (2016). A numerical investigation of the wake of an axisymmetric body with appendages. *Journal of Fluid Mechanics*, 792, 470-498.
- Posa, A., & Balaras, E. (2020). A numerical investigation about the effects of Reynolds number on the flow around an appended axisymmetric body of revolution. *Journal of Fluid Mechanics*, 884, A41.
- Spedding, G. R. (1997). The evolution of initially turbulent bluff-body wakes at high internal Froude number. *Journal of Fluid Mechanics*, 337, 283-301.
- Spedding, G. R. (2014). Wake signature detection. *Annual review of fluid mechanics*, 46(1), 273-302.
- Zheng, M., Liu, Y., Wang, Y., & He, Y. (2023). Simulation and experimental research on hydrodynamic performance of fully attached submarine in the surface and near the surface modes. *Ocean Engineering*, 281, 114785.